https://doi.org/10.5194/egusphere-2026-4158
Preprint. Discussion started: 18 August 2026


# River-induced circulations alter ozone distribution, source contributions, and chemical sensitivity in a river–valley city along the Yangtze River

Yan Lu [1], Yiming Guo [2], Yan Zhang [3], Min Shao [2,*]

[1] *College of Environmental Science and Engineering, Zhejiang University of Water Resources and Electric Power, Hangzhou 310018, China*

[2] *School of Environment, Nanjing Normal University, Nanjing 210046, China*

[3] *Hydrological Management Center of Zhejiang Province, Hangzhou 310009, China*

***Corresponding author:** E-mail: mshao@masonlive.gmu.edu (M. Shao)

https://doi.org/10.5194/egusphere-2026-4158
Preprint. Discussion started: 18 August 2026


**Abstract:** Ground-level ozone ($O_3$) pollution in river–valley cities is influenced by interactions among photochemistry, boundary-layer processes, and terrain-induced circulations, yet their combined effects on $O_3$ distributions remain insufficiently understood. Using WRF–CAMx coupled with source apportionment and process analysis, we investigated the three-dimensional distribution, source contributions, and formation characteristics of $O_3$ over the Nanjing section of the Yangtze River. The altitude of the $O_3$ maximum decreased from ~5.0 km in winter to ~2.0 km in summer, indicating stronger near-surface photochemical production and boundary-layer processes during warm seasons. Distinct spatial heterogeneity was observed between the river corridor and adjacent urban areas. Daytime near-surface $O_3$ development was weaker over the river in summer, whereas the high-$O_3$ layer extended downward to greater depths in spring and autumn. Regional background transport accounted for most total $O_3$, while suburban contributions increased during high-$O_3$ episodes, reaching 45.5% under $O_3$ concentrations of at least 160 μg/m$^3$ in July. Transport and diffusion associated with river-breeze circulations played important roles in regulating $O_3$ variability within the river corridor. $O_3$ formation remained volatile organic compound (VOC)-limited in spring and autumn, whereas river-breeze-induced nitrogen oxide (NO*x*) dilution shifted the river corridor to NO*x*-limited conditions approximately two hours earlier than in the surrounding urban area in summer. These findings indicate that river-induced circulations can substantially modify $O_3$ distributions, source contributions, and chemical sensitivity within river–valley cities, and that city-averaged and monthly mean characterizations may not fully capture local $O_3$ variability in complex terrain.

**Keywords:** Ozone vertical distribution, terrain-induced circulation, source apportionment, process analysis, river–valley region

https://doi.org/10.5194/egusphere-2026-4158
Preprint. Discussion started: 18 August 2026


## 1. Introduction

Air pollution episodes result from complex interactions between intensive anthropogenic emissions and meteorological conditions are harmful to the ecosystems and human health (Quimbayo-Duarte et al., 2021; Cheng et al., 2024; Lyu et al., 2025a). In recent years, ground-level ozone ($O_3$) has become an increasing environmental and public health concern due to its persistently high concentrations, especially in densely populated and industrialized urban areas (Zhang et al., 2025c; Tian et al., 2024; Zhang et al., 2023). Prolonged $O_3$ pollution episodes have been frequently observed in the Yangtze River Delta (YRD) and other major city clusters, where elevated precursor emissions coincide with stagnant synoptic conditions and strong photochemical activity (Liu et al., 2025; Wei et al., 2018; Xu et al., 2021; Gong et al., 2021; Mao et al., 2024). Understanding the mechanisms that govern $O_3$ formation and accumulation, particularly the interactions among chemical production, transport processes, and meteorological modulation within complex terrain, is critical for identifying terrain-specific drivers that enhance $O_3$ accumulation.

Tropospheric $O_3$ is a secondary pollutant formed through nonlinear photochemical reactions involving precursors such as nitrogen oxides ($NO_x$) and volatile organic compounds (VOCs). The rate and efficiency of $O_3$ formation are strongly regulated by meteorological factors, including ambient temperature, solar radiation, humidity, and wind speed and direction (Huszar et al., 2021; Qi et al., 2024). Consequently, $O_3$ exhibits strong spatial and temporal variability, particularly in regions with complex terrain and terrain-induced atmospheric circulations (Lu et al., 2022; Li et al., 2023; Zhang et al., 2025b).

Large river–valley regions present unique atmospheric environments where intensive anthropogenic emissions interact with dynamic meteorological processes shaped by the underlying terrain (Guo et al., 2024). The Yangtze River, the longest river in China, forms an extensive river–valley system that significantly modulates local boundary layer structures and atmospheric transport pathways. Unlike typical urban plains, regions along the Yangtze River, such as the Nanjing river section, are influenced by land-water thermal contrasts, topographic channeling, and river-breeze

https://doi.org/10.5194/egusphere-2026-4158
Preprint. Discussion started: 18 August 2026


circulations. These processes can enhance near-surface accumulation and vertical stratifications of pollutants, including particulate matter and NO*x* (Shao et al., 2024b; Qi et al., 2024). Terrain-driven circulations, combined with enhanced photochemical activity during the warm season, are likely to influence the frequency and intensity of $O_3$ pollution events, although the quantitative mechanisms for $O_3$ specifically remain unclear.

Nanjing is located at a key bend of the Yangtze River and is surrounded by low mountains on three sides, creating a diverse and dynamic meteorological environment. The interplay among river breezes, mountain–valley winds, urban heat island circulations, and complex distributions of anthropogenic and biogenic emissions leads to spatial heterogeneity in $O_3$ formation and vertical distribution. In addition to local emissions, regional-scale transport and in situ chemical transformations play important roles in the accumulation and persistence of $O_3$ (Li et al., 2021; Hou et al., 2024). Under stagnant meteorological conditions with strong solar radiation and weak boundary layer mixing, $O_3$ can accumulate over extended periods and across large areas (Zhang et al., 2025c; Shi et al., 2021; Li et al., 2021), conditions that frequently occur in the YRD (Qi et al., 2024; Shi et al., 2021; Xu et al., 2021) and complicate the assessment of source contributions and pollution formation mechanisms. Furthermore, the vertical distribution of $O_3$ is strongly influenced by boundary layer structure, turbulence, and local circulations (Li et al., 2023; Zhang et al., 2025a), and terrain-induced circulations in river–valley regions may further modulate vertical $O_3$ profiles, affecting the timing and magnitude of peak surface $O_3$ events (Guo et al., 2024). However, the specific mechanisms through which these terrain-induced meteorological processes regulate $O_3$ generation efficiency and vertical structure have not been sufficiently elucidated.

While prior studies have investigated $O_3$ pollution at the regional scale across the YRD (Zhang et al., 2025c; Wu and An, 2025; Lyu et al., 2025b; Mao et al., 2024; Gong et al., 2021; Shi et al., 2021; Wang et al., 2022), relatively few have systematically examined how terrain-induced meteorological processes, especially vertical exchange, affect $O_3$ distribution within specific subregions such as Nanjing. In particular, the interplay between complex topography, mesoscale circulations, and precursor

https://doi.org/10.5194/egusphere-2026-4158
Preprint. Discussion started: 18 August 2026


emissions remains an open question with important implications for air quality management and policy design.

To better understand the formation mechanisms and key influencing factors of $O_3$ pollution in this region, this study employs the Comprehensive Air Quality Model with Extensions (CAMx) to simulate $O_3$ pollution over the Nanjing section of the Yangtze River. By integrating source apportionment (SA) and process analysis (PA) techniques, we aim to elucidate the roles of meteorological and photochemical processes in shaping the spatiotemporal characteristics of $O_3$ pollution in this topographically complex region.

## 2. Materials and methods

This study focuses on the Nanjing section of the lower Yangtze River. This segment of the river flows through Nanjing from the southwest to the northeast before turning eastward, with an average width of approximately 1.2 km and a maximum width of about 2 km. The urban core of Nanjing is located to the southeast of the river, while multiple industrial parks are distributed along both riverbanks, which are later designated as source regions in the model configuration (Figure 1). Nanjing's prevailing winds are typically easterly during the warm season and northerly in the cold season, which can influence regional pollutant transport (Song and Shao, 2023). The surrounding terrain is characterized by Mt. Laoshan to the west and Mt. Ningzhen to the east, with elevations reaching up to 442 m. This complex topography plays a critical role in shaping local airflow patterns and the dispersion of air pollutants (Song and Shao, 2023).

https://doi.org/10.5194/egusphere-2026-4158
Preprint. Discussion started: 18 August 2026


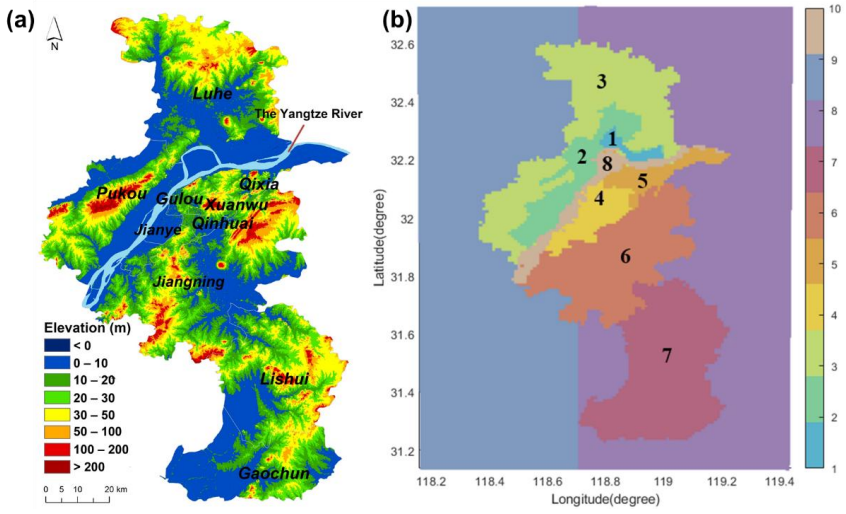


**Figure 1.** Terrain of the study area and source regions in CAMx. Region 1: Industrial park in Jiangbei New Area, north of the Yangtze River; Region 2: Remaining part of Jiangbei New Area (excluding Region 1), a national-level industrial zone; Region 3: Pukou and Luhe districts, north of the Yangtze River (excluding Regions 1 and 2); Region 4: Urban core of Nanjing (Gulou, Xuanwu, Qinhuai, and Jianye districts); Region 5: Education district with an industrial park (Qixia district), south of the Yangtze River; Region 6: Jiangning district, a suburban area with multiple campuses and industrial parks; Region 7: Outer suburbs of Nanjing (Lishui and Gaochun district); Region 8: Nanjing section of the Yangtze River.

The Advanced Core of the Weather Research and Forecasting (WRF, version 4.3; Skamarock et al., 2019) was used to provide meteorological fields for the CAMx chemical transport model. Initial and boundary conditions for WRF simulation were obtained from the NCEP FNL global analysis data (0.25° horizontal resolution, 26 vertical levels; https://doi.org/10.5065/D65Q4T4Z). Three nested domains were configured, with the innermost domain set to a horizontal resolution of 1 km, considering the ~2 km width of the Nanjing section of the Yangtze River and the recommended lower limit for planetary boundary layer parameterization (Sueki et al., 2019). To improve terrain representation, the 90 m Shuttle Radar Topography Mission (SRTM-3) dataset (https://lpdaac.usgs.gov/) was used to replace the default WRF

https://doi.org/10.5194/egusphere-2026-4158
Preprint. Discussion started: 18 August 2026


topography and was interpolated to the inner domain. Spectral nudging (Von Storch et al., 2000) was applied to wind fields above the planetary boundary layer using a wavenumber of 4 in both zonal and meridional directions, allowing large-scale (>1000 km) features to be constrained. A nudging coefficient of $3.0 \times 10^{-4}$ was used. Further details on domain configuration and parameterizations are available in Shao et al. (2024b).

The CAMx simulations employed the same domain structure as the WRF model, with three additional buffer grids added to the nested domains (D2 and D3) to handle internal lateral boundary conditions. The chemical mechanisms employed include CB05 for gas-phase chemistry, RADM-AQ for aqueous processes, ISORROPIA for inorganic thermodynamics, a fine/coarse aerosol scheme, and SOAPv2.2 for secondary organic aerosol formation. Anthropogenic emissions were compiled from multiple sources with varying resolutions: the Multi-resolution Emission Inventory for China for the year 2017 (MEIC, 0.25°, Zheng et al., 2014; Li et al., 2017), the Jiangsu provincial inventory (2017, ~3 km), and the Nanjing local inventory (2018, ~1 km). Emission merging followed a hierarchical approach, using MEIC as the base while replacing corresponding grid cells with Jiangsu and Nanjing data. A 5 × 5 filter was applied along administrative borders to smooth transitions. MEIC emissions, treated as area sources, were provided as monthly sectoral data, while the Jiangsu and Nanjing inventories included detailed point-source information for industry and power plants and were treated accordingly. The annual emissions from Jiangsu and Nanjing were temporally allocated to monthly values using MEIC-derived ratios. To match CAMx input requirements, NO*x* was split into NO and $NO_2$ (85%/15%), $PM_{2.5}$ was apportioned into sulfate, nitrate, and primary inorganic matter (26%/14%/60%) (Dai et al., 2019; Luo et al., 2023), and total VOCs were mapped to CB05 species using MEIC profiles due to a lack of local VOC speciation. Biogenic emissions were generated using the Model of Emission of Gases and Aerosols from Nature (MEGAN; Guenther et al., 2006, 2012).

To investigate the formation mechanisms of $O_3$, the CAMx model was applied with integrated SA and PA tools. The SA module quantifies the contributions of different source regions, sectors, and precursors (e.g., NO*x* and VOCs) to ambient $O_3$

https://doi.org/10.5194/egusphere-2026-4158
Preprint. Discussion started: 18 August 2026


concentrations, while the PA module, comprising integrated process rate (IPR) and chemical process analysis (CPA), assesses the roles of key physical and chemical processes in $O_3$ production and depletion. Model simulations were conducted for four representative months in 2019 (January, April, July, and October), which represent winter, spring, summer, and autumn, respectively, with the configuration, input data, and evaluation procedures consistent with our previous study (Shao et al., 2024b).

The spatial distribution of NO*x*, VOC, CO, and $PM_{2.5}$ emissions in Nanjing is provided in the Supplementary Materials (Figure S1). Among these pollutants, NO*x* and VOC are the primary precursors of tropospheric $O_3$, while CO also contributes to $O_3$ formation through HO*x* cycling. $PM_{2.5}$ is additionally included to present co-emitted pollutants from combustion-related sources and to provide context for emission patterns associated with $O_3$ precursors. Region 1 (Jiangbei industrial park) was the dominant source of VOC emissions, accounting for 62% of the citywide total. This highlights the strong potential for localized $O_3$ production driven by industrial activities emitting highly reactive VOC species. Although biogenic emissions, estimated using the MEGAN model, are present across the study domain, they are substantially lower than anthropogenic sources, particularly in Region 1. As a result, the annual VOC emissions in Region 1 significantly exceeded those of the other pollutants involved in different atmospheric chemical processes (Shao et al., 2024b). Region 4 (urban core) contributed 29% of NO*x* and 34% of VOC emissions, consistent with intense vehicular traffic and energy consumption, and forming a key $O_3$ precursor mix in densely populated areas. Region 8 (Yangtze River corridor) emitted 14% of NO*x*, reflecting combustion-dominated activities such as shipping and port operations. Although VOC emissions in Region 8 were relatively low (4%), the elevated NO*x* levels may support $O_3$ formation under certain atmospheric conditions, particularly in downwind or transition zones. Overall, the spatial mismatch between NO*x* and VOC emissions across different functional zones suggests that $O_3$ formation regimes in Nanjing are likely to be spatially heterogeneous, which is consistent with our previous findings (Shao et al., 2024a).

## 3. Results and discussion

https://doi.org/10.5194/egusphere-2026-4158
Preprint. Discussion started: 18 August 2026


### 3.1 Model validation

The model performance was evaluated according to the established protocols of our previous studies (Shao et al., 2024b), which have demonstrated the reliability of the meteorological fields as well as the model configuration. In this study, the daily maximum 8-hour moving average (MDA8) $O_3$ concentrations simulated by the model were compared with observed values from nine monitoring stations across Nanjing, most of which are located in densely populated urban districts (Figure 1). Mean bias (Bias) and root mean square error (RMSE) were used to evaluate the performance of the model's ability in capturing MDA8 in four representative months (Figure S2).

In January, the model shows the best agreement with observations, with a Bias of 4.86 μg/m$^3$ and an RMSE of 21.43 μg/m$^3$, indicating high reliability during winter. Moderate overestimations are found in April (Bias = 13.82 μg/m$^3$, RMSE = 32.94 μg/m$^3$) and July (Bias = 6.13 μg/m$^3$, RMSE = 36.85 μg/m$^3$), while a slight underestimation occurs in October (Bias = −11.29 μg/m$^3$, RMSE = 29.56 μg/m$^3$). Overall, the biases remain within ±15 μg/m$^3$, and RMSE values are within 20–40 μg/m$^3$, suggesting that the model can reasonably reproduce the day-to-day variation and seasonal characteristics of MDA8 $O_3$ over Nanjing. This level of performance provides a reliable basis for subsequent source apportionment and process analysis.

### 3.2 Spatial distribution of simulated $O_3$ and meteorological factors

Gridded and regional averages of monthly mean $O_3$ concentrations across Nanjing are shown in Figure 2, revealing distinct spatial patterns. In January and October, $O_3$ concentrations are generally higher along the northern bank of the Yangtze River than along the southern bank. In contrast, in April and July, $O_3$ concentrations along the southern bank are slightly higher than those on the northern bank. During these warmer months, $O_3$ concentrations increase across most regions, with the urban core (Region 4) exhibiting the highest concentrations, reaching a monthly mean MDA8 of about 130 μg/m$^3$ in July. Suburban and industrial zones (Regions 1–3) show moderately elevated $O_3$ levels. Such disparate seasonal patterns over the two banks of the Yangtze River may reflect potential impacts from background wind fields, local thermal

https://doi.org/10.5194/egusphere-2026-4158
Preprint. Discussion started: 18 August 2026


circulations and emission distribution.

Furthermore, distinct $O_3$ distributions are observed across different underlying surfaces. The Yangtze River surface (Region 8) generally shows lower $O_3$ concentrations than surrounding land areas, particularly in October, which may be related to higher surface humidity, insufficient precursors, and weaker photochemical activity over water. The mountainous area (Region 6) exhibits slightly higher $O_3$ concentrations than the urban core in most months, possibly due to lower anthropogenic emissions of NO*x* that reduce $O_3$ consumption and large natural emissions of biogenic VOCs that increase $O_3$ formation.

Some meteorological factors, including 10 m wind speed (WS10), 2 m relative humidity (RH2), and planetary boundary layer height (PBLH) over the study domain were analyzed in our previous study (Shao et al., 2024b). The current study expands the analysis by incorporating additional meteorological factors, such as 2 m air temperature (T2), daily maximum 2 m air temperature (max T2), downward shortwave radiation (SW), and RH2 (Figure S3). July was chosen as the representative summer month for analysis due to its typical summer characteristics, including higher temperatures, stronger solar radiation, and more pronounced photochemical reactions, making it a key month for studying $O_3$ concentration variability.

RH2 is an important meteorological factor influencing $O_3$ concentrations, as higher humidity can suppress photochemical reactions and promote $O_3$ deposition. Notably, RH2 along the Yangtze River surface is substantially higher than in other regions, exceeding the Nanjing average by 5.8-14.2% and the urban core (Region 4) by 21.5-31.8% across the four months. The differences in PBLH across regions play a crucial role in $O_3$ vertical distribution and surface accumulation, which will be further discussed in the context of vertical profiles in the following section. The urban core has the highest PBLH (535 m), which promotes stronger vertical mixing and the upward dispersion of both $O_3$ and its precursors, thereby diluting surface $O_3$ concentrations to some extent. Nevertheless, the abundant precursor emissions and high temperatures in the urban core still result in the highest $O_3$ levels among all regions. In contrast, the Yangtze River (Region 8) has the lowest PBLH (360 m), which limits vertical dilution

https://doi.org/10.5194/egusphere-2026-4158
Preprint. Discussion started: 18 August 2026


and supports pollutant accumulation near the surface. Industrial areas (Regions 1 and 2) exhibit moderately high PBLH values (462–471 m), which, combined with elevated temperatures, create typical $O_3$ hotspots. Notably, Region 3, despite having relatively low temperatures (27.7 °C), also has a low PBLH (434 m), which may limit vertical mixing and contribute to higher surface $O_3$ concentrations despite weaker photochemical conditions.

Interestingly, the Yangtze River (Region 8) records the second-highest average $O_3$ concentration in July, slightly lower than the urban core and 2.8% higher than the citywide average. In contrast, during other months, Region 8 consistently shows significantly lower $O_3$ concentrations than the citywide average, with the lowest monthly mean $O_3$ levels in January (22.3 $\mu g/m^3$). These patterns may be influenced by local meteorological and topographical conditions, as will be further discussed in the context of source apportionment in Section 3.4. Specifically, Region 8 has significantly higher RH2 and WS10 than other regions, but a much lower PBLH (Shao et al., 2024b). For instance, RH2 is 7.8–14.2% higher than the city average and 21.1–31.8% higher than the urban core; WS10 is 11.1–21.2% higher than the city average and 23.6–38.0% higher than the urban core. These meteorological conditions could prevent the formation and enhance the transport of $O_3$. In contrast, PBLH is the lowest over the river which is conducive to the accumulation of air pollutants.

$O_3$ accumulation in Region 8 may also be influenced by local thermal circulations generated by the river, surrounding urban areas, and topography. Previous studies (e.g., Shao et al., 2024a) suggest that the thermal circulation over the river and its northwest side is relatively weak, embedded within the dominant urban heat island circulation. This configuration likely enhances subsidence over the river while enhancing upward motion in the urban core. Combined with the lower PBLH over the river and geostrophic wind patterns, these factors may limit both horizontal and vertical dispersion, favoring $O_3$ accumulation during the summer. In other seasons, strengthening northerly winds and increased land–river temperature differences may enhance dispersion over the river corridor, potentially contributing to the lower $O_3$ concentrations observed in October.

https://doi.org/10.5194/egusphere-2026-4158
Preprint. Discussion started: 18 August 2026


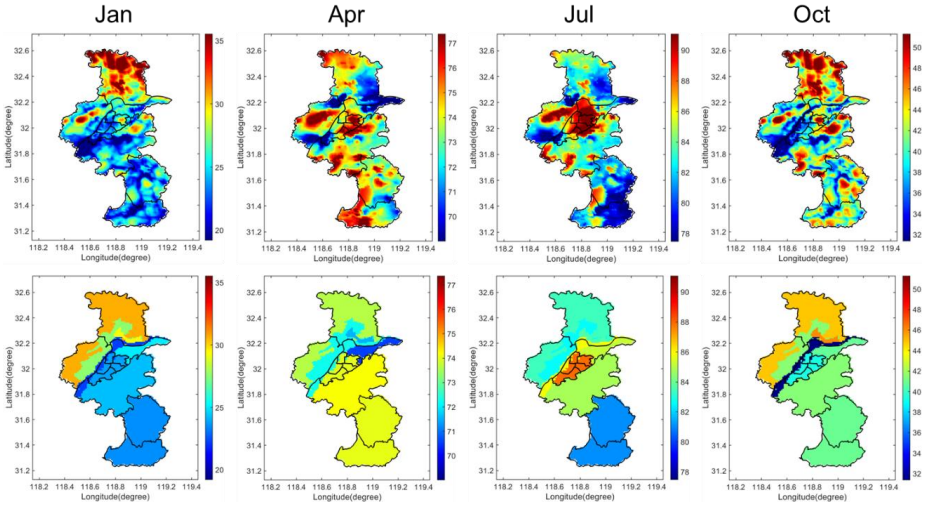


**Figure 2.** Monthly mean $O_3$ concentrations (first row, ug/m$^3$) and regional average $O_3$ levels (second row, ug/m$^3$) for each region defined in Figure 1.

### 3.3 Vertical distribution characteristics of $O_3$

Based on the simulation results, the domain averaged vertical $O_3$ profiles over the Nanjing section of the Yangtze River exhibits pronounced seasonal variability (Figure 3). Besides the relatively consistent increase in $O_3$ concentrations with altitude within the lower troposphere, the $O_3$ maximum shows a clear downward propagation from winter to summer. In January, $O_3$ concentration reaches a broad peak of ~85 μg/m$^3$ at ~5.0 km; in April and July, the peaks descend to ~2.7 km (106.1) and ~2.0 km (113.7 μg/m$^3$), respectively; in October, an intermediate peak of ~95.1 μg/m$^3$ occurs at ~3.5 km. Unlike the double-maxima vertical structure reported by Chen et al. (2023) for coastal southern China, our simulated summer $O_3$ profile over the Nanjing section shows a single pronounced peak at ~2.0 km, likely reflecting differences in boundary layer dynamics between inland Nanjing and coastal southern China. Above approximately 5–6 km, $O_3$ concentrations in spring, summer, and autumn are relatively close within a range of ~91–96 μg/m$^3$, with little seasonal differentiation. Below this altitude, however, the profiles diverge markedly, with a difference of up to ~24 μg/m$^3$ at 2.1 km (Jul: 113.7 vs. Oct: 89.5 μg/m$^3$), highlighting the dominant role of near-

https://doi.org/10.5194/egusphere-2026-4158
Preprint. Discussion started: 18 August 2026


surface photochemical production and boundary layer dynamics in driving warm-season $O_3$ accumulation.

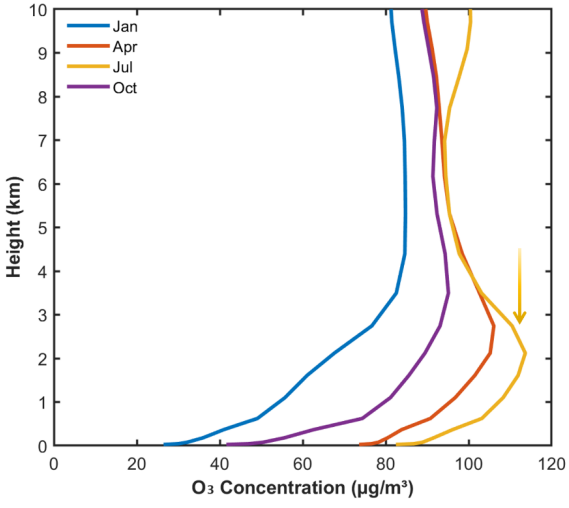


**Figure 3.** Vertical profiles of domain-averaged $O_3$ concentrations for January, April, July, and October.

During summer, intense solar radiation drives active photochemical $O_3$ formation within the boundary layer, while a deeper and more turbulent mixing layer facilitates vertical redistribution, resulting in a pronounced $O_3$ maximum at ~2 km. During winter, suppressed photochemical activity and a shallow, stable boundary layer reduce near-surface $O_3$ concentrations. Meanwhile, the collapse of the nocturnal boundary layer isolates the residual layer from the surface, allowing $O_3$ to accumulate aloft and be gradually transported into the free troposphere, producing a broad and relatively uniform $O_3$ distribution throughout the mid-troposphere (Zhang et al., 2021).

The diurnal evolution of $O_3$ anomalies (hourly concentration minus daily mean) as a function of altitude for January, April, July, and October is provided in the Supplementary Materials (Figure S4). A consistent diurnal pattern is observed in all seasons, characterized by negative anomalies during nighttime and early morning and positive anomalies during the daytime. However, substantial seasonal differences are evident in the intensity, vertical extent, and temporal evolution of the anomaly field.

In January and October, the strongest positive and negative anomalies are concentrated within the lower troposphere, with the amplitude of the diurnal cycle

https://doi.org/10.5194/egusphere-2026-4158
Preprint. Discussion started: 18 August 2026


decreasing rapidly with height. In January, a notable feature is the persistent positive anomaly between 1 and 2 km throughout much of the day, likely reflecting $O_3$ retention within the residual layer where vertical mixing is suppressed under stable wintertime conditions. In contrast, the influence of vertical exchange on the diurnal $O_3$ cycle becomes much more pronounced in April and July. The anomaly signal extends to nearly 3 km in April and exceeds 4 km in July, accompanied by substantially larger anomaly magnitudes. These results indicate that the vertical extent of diurnal $O_3$ variability increases markedly during the warm season.

Another notable feature is the altitude-dependent timing of the anomaly transition. In July, the $O_3$-anomaly boundary exhibits a clear upward tilt, with the transition from negative to positive anomalies occurring earlier near the surface and progressively later at higher altitudes. Meanwhile, the positive anomaly core first develops in the lower atmosphere and subsequently expands upward. This increasing phase lag with height suggests that the diurnal $O_3$ signal is initiated near the surface and gradually propagates to higher altitudes. In comparison, the tilt of the zero-anomaly boundary is much weaker in January and October, indicating a more limited vertical development of the diurnal $O_3$ cycle. In addition, the persistence of weak positive anomalies in the middle and upper layers during daytime in January implies that $O_3$ variability differs substantially between the lower and upper atmosphere. Overall, the warm season is characterized not only by larger anomaly amplitudes but also by more pronounced vertical expansion and altitude-dependent phase shifts, reflecting a more complex vertical structure of the diurnal $O_3$ cycle.

Figure 4 presents the seasonal diurnal vertical profiles of $O_3$ concentration over different regions (the Yangtze River and surrounding typical regions in Nanjing are selected for analysis). Overall, all regions exhibit a consistent vertical structure across the four seasons, with higher $O_3$ concentrations in the upper layers (1–2.5 km) and lower concentrations near the surface (0–0.5 km). Near-surface $O_3$ increases during daytime in association with boundary layer development and decreases at night. In terms of regional differences, the vertical development of near-surface $O_3$ over the Yangtze River reach (Region 8) during daytime was notably weaker than that over the

https://doi.org/10.5194/egusphere-2026-4158
Preprint. Discussion started: 18 August 2026


surrounding urban areas in July, possibly related to the relatively slow daytime warming of the river surface and the associated weaker boundary layer development. In April and October, the high-value $O_3$ layer over the river region extended downward to greater depths compared to the surrounding urban areas, suggesting a continued modulating effect of land–river thermal contrasts on the vertical $O_3$ structure beyond summer. In January, the vertical $O_3$ profiles across all regions became more uniform with the smallest inter-region differences, which is consistent with the expected overall lower $O_3$ concentrations, reduction in land–river thermal contrasts and local circulation intensity during winter. These features suggest that local thermal circulation may be one of the important factors governing the seasonal differences in the vertical distribution of $O_3$ over the Yangtze River reach in Nanjing. These systematic differences between the river corridor and the surrounding urban areas indicate that surface-based or city-averaged analyses may not fully characterize the spatial and vertical heterogeneity of $O_3$ in river–valley urban environments, particularly during summer when the land–river contrast is strong.

https://doi.org/10.5194/egusphere-2026-4158
Preprint. Discussion started: 18 August 2026


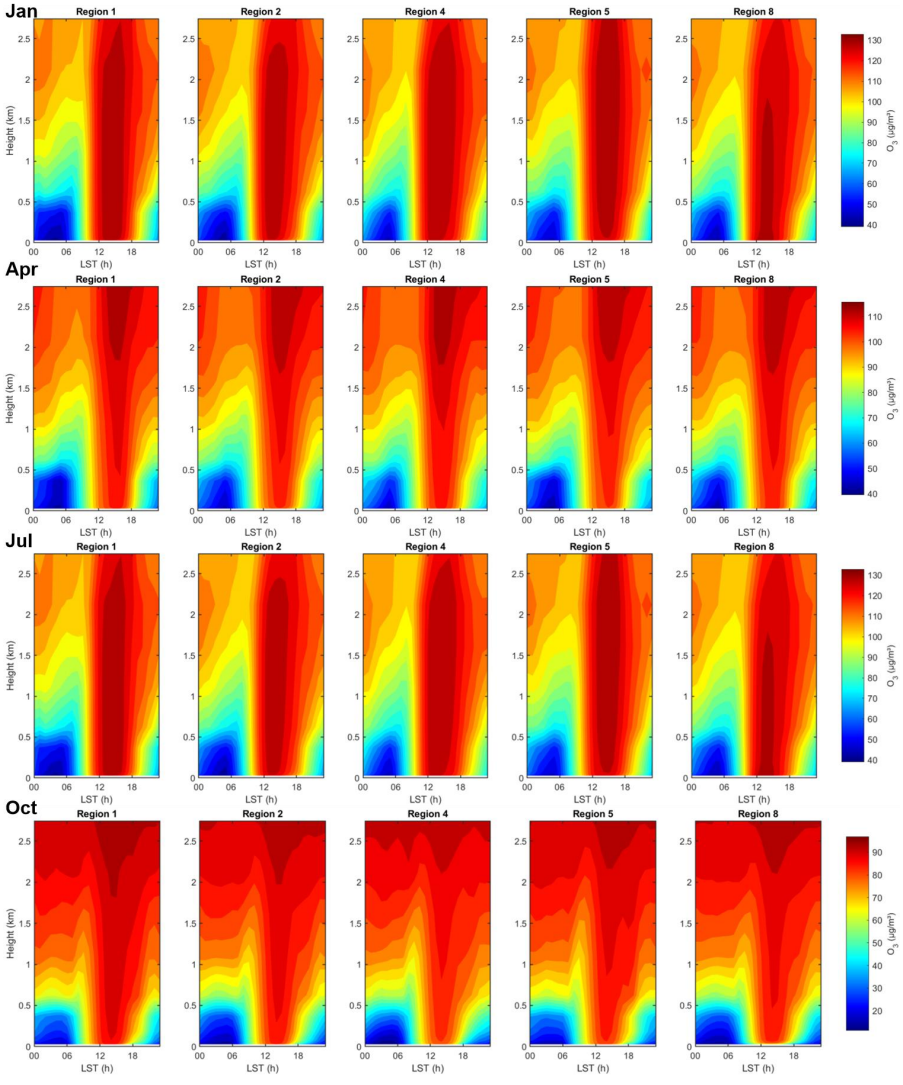


**Figure 4.** Seasonal diurnal vertical profiles of $O_3$ concentration over the Yangtze River and surrounding typical regions in Nanjing (January, April, July, and October).

To investigate the influence of topography and local circulations on the vertical distribution of $O_3$, we compared two cross-sections in Nanjing: a latitudinal transect at 32.032°N crossing the Yangtze River, the Ningzhen-Laoshan mountain system and urban core, and a longitudinal transect at 118.842°E crossing the Jiangbei industrial park, the Yangtze River, and Mt. Zijin, using the monthly mean wind fields from July

https://doi.org/10.5194/egusphere-2026-4158
Preprint. Discussion started: 18 August 2026


(Figure 5).

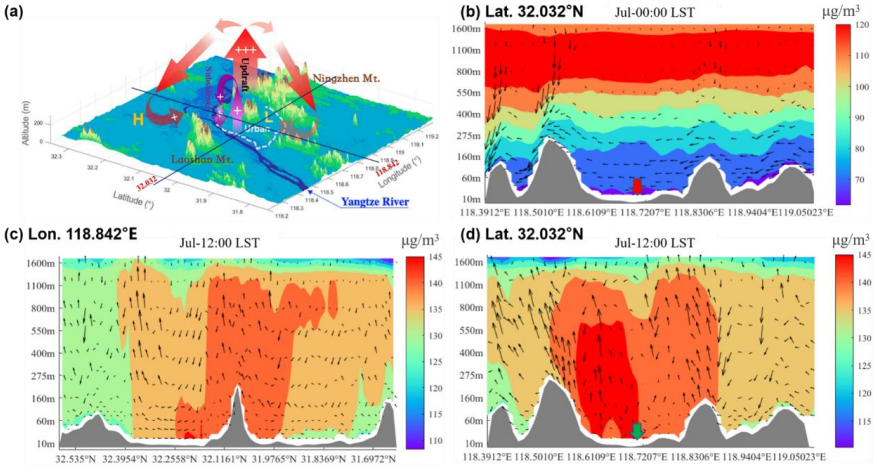


**Figure 5.** Topographic context and vertical $O_3$ distributions (μg/m$^3$) along cross-sections in Nanjing. (a) Regional terrain and schematic local circulations (Shao et al., 2024b); (b) July 00:00 LST at 32.032°N, showing nocturnal near-surface $O_3$ depletion under a stable, subsiding boundary layer and an elevated residual $O_3$ layer aloft (red arrow marks the Yangtze River); (c) July 12:00 LST at 118.842°E, showing moderate near-surface $O_3$ in the Jiangbei industrial sector, a pronounced vertical $O_3$ maximum over the Yangtze River and terrain-induced upslope lifting over Mt. Zijin; (d) July 12:00 LST at 32.032°N, highlighting a 0.4–1.0 km elevated $O_3$ layer driven by strong updrafts and a vertical $O_3$ high-value column at the green-arrow location.

At night along the latitudinal transect (Figure 5b, Jul-00:00 LST), near-surface $O_3$ concentrations are markedly suppressed (~70–80 μg/m$^3$), with a pronounced depletion pocket near 118.63°E (red arrow) likely reflecting strong nocturnal NO*x* titration under a stable, shallow boundary layer with weakened ventilation, as illustrated by the relatively weak east wind below 400 m, which could be the result of the combined effect from local thermal circulations shown in Figure 5(a). $O_3$ increases steeply with height, reaching ~110–120 μg/m$^3$ above 800 m within the residual layer, consistent with the suppression of vertical mixing and the absence of photochemical production at night.

During daytime along the same latitudinal transect (Figure 5d, Jul-12:00 LST), the

https://doi.org/10.5194/egusphere-2026-4158
Preprint. Discussion started: 18 August 2026


$O_3$ vertical structure is fundamentally altered by active local circulations. A persistent elevated $O_3$ layer (~135–145 μg/m$^3$) develops between 0.4 and 1.0 km, driven by intense photochemical production and strong updrafts that transport precursors aloft, as reflected by the pronounced upward wind vectors. At the green-arrow location, near-surface $O_3$ (~130–135 μg/m$^3$) extends upward into a distinct vertical high-value column, consistent with concentrated convective lifting at that position.

Along the longitudinal transect at 118.842°E (Figure 5c, Jul-12:00 LST), near-surface $O_3$ in the northern sector (Region 1 and Region 3, ~32.4–32.5°N) remain relatively moderate (~120–125 μg/m$^3$), which may reflect the competing effects of photochemical $O_3$ production and NO*x*–VOC titration near the Jiangbei industrial emission sources. A striking near-surface $O_3$ maximum (~145 μg/m$^3$) is observed over the Yangtze River and Baguazhou Island (~32.26°N), forming a pronounced vertical high-value column extending from the surface to above 1000 m, driven by local upward transport as evidenced by the strong upward wind vectors at this location. Further south, the topographic rise of Purple Mountain generates vigorous daytime upslope winds predominantly on its northern flank, as evidenced by the upward wind vectors, lifting $O_3$-rich air from the lowlands to the north and contributing to elevated concentrations aloft. The broad southern sector (Regions 5 and 6, south of 32°N) exhibits a persistently high $O_3$ layer (~135–140 μg/m$^3$) extending through the mid-troposphere, consistent with active photochemical production and strong convective mixing under daytime heating.

Comparing Figures 5(b) and 5(d) reveals a striking diurnal reversal at 32.032°N: the nocturnal profile is characterized by surface depletion beneath a high-$O_3$ residual layer, whereas the daytime profile shows an active elevated $O_3$ accumulation layer fed by convective uplift. Comparing Figures 5(c) and 5(d) highlights the contrasting roles of different local forcing mechanisms at the same local noon: the longitudinal transect (5c) reveals how industrial emissions, local upward transport, and upward transport jointly shape a pronounced near-surface $O_3$ maximum over Baguazhou, while the latitudinal transect (5d) features a more horizontally uniform elevated layer driven by strong updrafts and convective lifting over the urban core. Together, these contrasting

https://doi.org/10.5194/egusphere-2026-4158
Preprint. Discussion started: 18 August 2026


patterns demonstrate that the interplay of nocturnal stability, river breezes, urban updrafts, and terrain-induced flows plays a critical role in shaping the vertical and horizontal heterogeneity of $O_3$ across Nanjing.

### 3.4 $O_3$ transport revealed through source apportionment technology

The monthly mean local source contributions (excluding contributions from regions outside Nanjing) provide useful information on the influence of local circulations on $O_3$ accumulation and redistribution within the Yangtze River corridor (Figure 6). It should be noted that the source contributions discussed here refer to the locally attributed fraction only, which accounts for 12.8%, 44.9%, 59.2%, and 23.9% of total $O_3$ in January, April, July, and October, respectively, with the remainder dominated by regional background transport. Within this local fraction, the highest contribution from Region 8 occurs in April, exceeding 60%. Because Region 8 represents the river corridor rather than a major industrial emission area, this elevated contribution likely reflects favorable meteorological conditions for $O_3$ retention within the river corridor rather than stronger local emissions. Favorable spring meteorological conditions, including increasing solar radiation and relatively weak atmospheric dispersion, may further enhance the retention of $O_3$ within the river corridor. During the 14:00 period, when photochemical activity is the strongest, the contribution from Region 8 increases further, reaching 65.2% in April and 59.7% in July, indicating enhanced daytime $O_3$ formation within the river corridor.

Seasonal variations are particularly pronounced. In winter, $O_3$ concentrations are primarily influenced by northerly winds that transport $O_3$ and its precursors from the industrial areas north of the river, with monthly mean contributions from Region 1 and Region 2 reaching 18.7% and 15.5%, respectively, together accounting for over a third of the locally attributed $O_3$. Contributions from the urban area (Region 4) and southern Qixia (Region 5) are comparatively modest, at around 9–11%. In spring, Region 8 becomes overwhelmingly dominant, while contributions from the northern industrial regions (Region 1–3) decline markedly compared to winter, suggesting a seasonal shift in large-scale circulation patterns from north wind to easterlies. In summer, stronger

https://doi.org/10.5194/egusphere-2026-4158
Preprint. Discussion started: 18 August 2026


photochemical activity sustains a high river surface contribution (56.9%), though enhanced vertical mixing and dispersion slightly reduce its relative share compared to spring. In autumn, the river surface contributes 26.4%, with Qixia (Region 5) and Jiangning (Region 6) accounting for 11.2% and 15.5%, respectively, reflecting a more dispersed source pattern under transitional circulation conditions.

Pronounced diurnal differences are also observed across all seasons, likely reflecting the influence of thermally driven local circulations. During the daytime, the local contribution from Region 8 itself is largest, reaching 31.5% in January and 60.1% in July, indicating that $O_3$ over the river is then dominated by local-scale processes, with cross-bank transport from surrounding regions contributing a correspondingly smaller share. At night, this local fraction drops markedly to 12.8% in January and 39.3% in July, and the contributions from the regions on both banks rise accordingly, indicating an increased role of transport from riverside source areas to the river receptor. In January, the nighttime contributions to Region 8 from Pukou and Luhe (Region 3), southern Qixia (Region 5), and Jiangning (Region 6) rise to 12.3%, 14.9%, and 9.5%, respectively, consistent with radiative cooling and boundary layer stabilization near emission sources. In July, the nighttime contributions to Region 8 from Region 3 and Region 6 increase to 4.6% and 15.0%, reflecting nocturnal accumulation under stable conditions and the possible terrain-induced recirculation. The transitional seasons of April and October exhibit the same diurnal regime, in which the local contribution over the river dominates during the daytime and the contributions from the regions on both banks rise at night, indicating that this pattern is a robust, year-round feature. These patterns suggest that thermally driven local circulations modulate the diurnal partitioning between local production over the river and transport from the regions along both banks, thereby shaping the source composition of $O_3$ within the Yangtze River corridor.

Under high $O_3$ concentration conditions, the influence of regional transport becomes more pronounced. In April, as $O_3$ concentrations increase, contributions from Jiangning (Region 6) and the suburban areas (Region 7) rise substantially from their monthly mean values of 5.3% and 2.4% to 14.8% and 23.3% under $\geq$120 $\mu g/m^3$

https://doi.org/10.5194/egusphere-2026-4158
Preprint. Discussion started: 18 August 2026


conditions, and remain elevated at 13.4% and 22.6% under ≥160 μg/m$^3$, while the river surface contribution declines from 61.1% to 20.9% and 19.5%, respectively. This shift suggests that elevated $O_3$ episodes in spring are associated with enhanced transport from southern and suburban source regions rather than local circulation within the river corridor. In July, under ≥160 μg/m$^3$ conditions, the suburban contribution (Region 7) rises substantially from its monthly mean of 4.4% to 45.5%, with Region 3 contributing 18.6% and the river surface declining from 56.9% to 15.1%; under ≥200 μg/m$^3$, Region 7 further increases to 48.4% while the river surface decreases to 3.6%, indicating that extreme summer $O_3$ pollution is driven primarily by enhanced regional transport. In October, under ≥160 μg/m$^3$ conditions, Qixia (Region 5) increases markedly from its monthly mean of 15.5% to 32.6%, with Region 6 at 8.6% and the river surface at 22.3%; under ≥200 μg/m$^3$, Region 5 further rises to 40.0%, with Region 6 at 9.3% and the river surface at 21.6%, indicating that autumnal high-$O_3$ episodes are largely driven by local and nearby emissions under confined circulation from southeasterlies to easterlies. Overall, the spatial and temporal variations in source contributions under high-pollution conditions highlight the importance of both terrain-induced local recirculation and enhanced regional transport in shaping $O_3$ accumulation along the Yangtze River corridor. These episode-dependent shifts in the dominant source regions indicate that source-contribution patterns derived from monthly mean conditions may not adequately represent the processes governing high-$O_3$ episodes. Source attribution and mitigation assessments should therefore account explicitly for pollution intensity and the associated changes in regional transport.

https://doi.org/10.5194/egusphere-2026-4158
Preprint. Discussion started: 18 August 2026


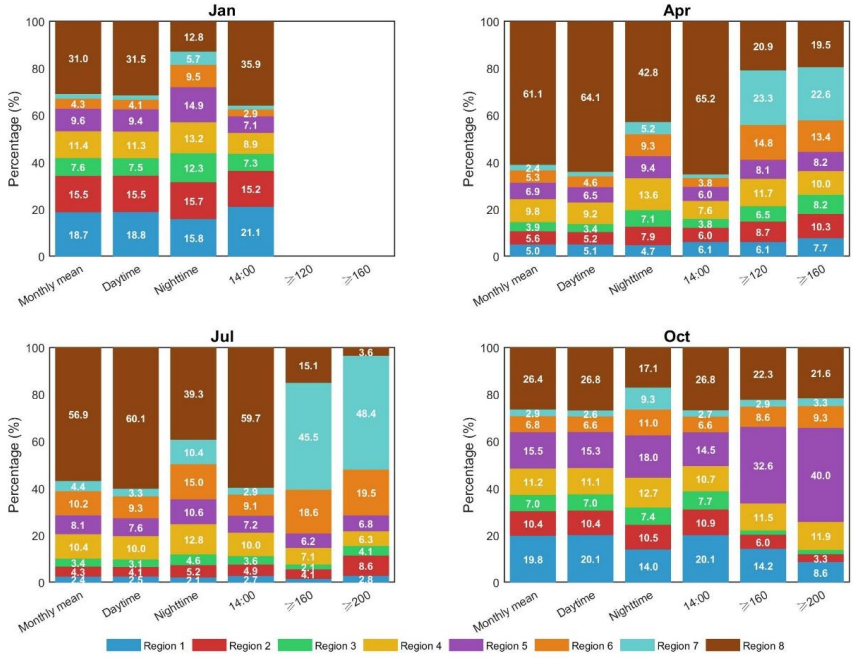


**Figure 6.** Monthly mean proportions (%) of local source contributions to $O_3$ along the Yangtze River (Region 8) under various conditions. The daytime period is defined as 08:00–18:59; nighttime includes both 00:00–07:59 and 19:00–23:59; 14:00 represents the monthly mean proportions of source contributions at 14:00 LST; ≥120, ≥160 and ≥200 correspond to hours when the observed $O_3$ concentrations are ≥120 μg/m$^3$, ≥160 μg/m$^3$ and ≥200 μg/m$^3$, respectively.

### 3.5 $O_3$ formation revealed through process analysis technology

To further elucidate the mechanisms responsible for the distinctive source-contribution characteristics over the Yangtze River corridor, process analysis was conducted to quantify the contributions of different chemical and transport processes to $O_3$ formation. The results indicate that the Yangtze River region of Nanjing (Region 8) exhibits distinct process characteristics compared with the city-wide mean (Region 1–5 and 8) (Figure 7). Diffusion processes show consistently positive differences across all seasons, consistent with the generally lower $O_3$ concentrations over the river corridor than in adjacent urban areas, which favor net diffusive transport toward the river region.

Vertical and horizontal advection exhibit coherent diurnal variations, highlighting

https://doi.org/10.5194/egusphere-2026-4158
Preprint. Discussion started: 18 August 2026


the influence of boundary layer evolution and river-induced local circulations on $O_3$ transport. Vertical advection shows positive differences during daytime and negative differences at night, indicating enhanced daytime exchange between the river corridor and the overlying atmosphere as the boundary layer develops. Horizontal advection displays a clear diurnal reversal, with negative differences from morning to early afternoon and positive differences from late afternoon through nighttime. This pattern is consistent with the daytime development and nighttime weakening or reversal of river-breeze circulation driven by land–river thermal contrasts.

Deposition processes exhibit positive differences, most prominently in summer, reflecting distinct surface characteristics and atmosphere–surface interactions over the river corridor compared with the surrounding urban environment. Gas-phase chemistry shows relatively small differences between the Yangtze River corridor and the city-wide mean across all seasons. This suggests that the distinct $O_3$ characteristics of the river region are associated primarily with differences in transport and diffusion processes driven by local circulations, rather than substantial differences in net chemical tendencies. These results highlight that topography-induced airflow and land–river interactions play a crucial role in shaping the $O_3$ budget over the Yangtze River region.

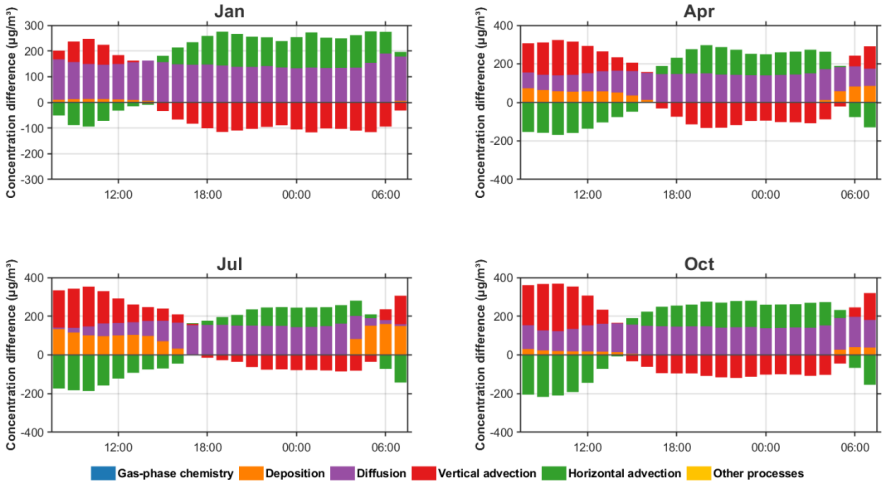


**Figure 7.** Differences in monthly mean diurnal $O_3$ concentration change rates: the Yangtze River (region 8) vs. average of regions 1–5 and 8 (excluding suburban areas) (LST, UTC+8).

https://doi.org/10.5194/egusphere-2026-4158
Preprint. Discussion started: 18 August 2026


The CPA approach was used to assess $O_3$ production sensitivity for April, July, and October. Daily CPA outputs from the CAMx model were used to calculate the production rates of $H_2O_2$ and $HNO_3$ ($P_{H_2O_2}/P_{HNO_3}$), which served as key indicators of $O_3$ production sensitivity. January was excluded from the diurnal analysis as near-zero $P_{H_2O_2}/P_{HNO_3}$ ratios throughout the day indicate negligible photochemical activity in winter, rendering the CPA-based sensitivity diagnosis uninformative for that season. Following thresholds adopted from previous studies (Li et al., 2022; Sillman, 1995; Vermeuel et al., 2019; Liu et al., 2025), regimes were classified as VOC-limited when $P_{H_2O_2}/P_{HNO_3}$≤0.25, transitional when 0.25–0.4, and NO*x*-limited when >0.4.

Figure 8 presents the diurnal variation of the monthly mean $P_{H_2O_2}/P_{HNO_3}$ ratio for Region 8 (Yangtze River corridor) and the urban mean (Regions 1–5) during the photochemically active period. In April and October, both Region 8 and the urban mean remain well below the VOC-limited threshold (0.25) throughout the day. In April, the two curves are nearly indistinguishable, with peak values of approximately 0.17 for both, confirming uniformly VOC-limited conditions with negligible influence from local circulations. In October, the urban mean peaks are slightly higher than Region 8 (~0.08 vs ~0.07), though both remain far below the sensitivity thresholds, indicating that local circulations exert minimal influence on regime differentiation in this season as well.

In contrast, July exhibits a pronounced diurnal pattern and a remarkable divergence between Region 8 and the urban mean. Both curves rise sharply after sunrise, but Region 8 peaks earlier (~12:00 LST, $P_{H_2O_2}/P_{HNO_3}$ > 1.0) and substantially exceeds the urban mean throughout the morning, with a maximum gap of 0.53 at 11:00 LST. The urban mean peaks later (~13:00 LST, ~0.6), remaining lower than Region 8 for most of the active period. Notably, Region 8 crosses the NO*x*-limited threshold (0.40) as early as 09:00 LST and sustains NO*x*-limited conditions until ~18:00 LST, while the urban mean crosses the same threshold approximately two hours later at 11:00 LST. This earlier and stronger sensitivity shift in Region 8 is consistent with the role of the

https://doi.org/10.5194/egusphere-2026-4158
Preprint. Discussion started: 18 August 2026


Yangtze River breeze: the onset of the river breeze in the late morning dilutes NO*x* concentrations along the river corridor, shifting the VOC/NO*x* balance toward NO*x*-limited conditions ahead of the broader urban area. The subsequent convergence of the two curves after ~18:00 LST, when the river breeze weakens, further supports this mechanism. The grey shading (12:00–18:00 LST) marks the peak photochemical period, during which the divergence between Region 8 and the urban mean is sustained, reinforcing the interpretation that local thermal circulations play a controlling role in modulating $O_3$ production sensitivity during summer.

Overall, $O_3$ production in Nanjing is primarily VOC-limited, but NO*x*-limited conditions emerge in summer, particularly in the Yangtze River corridor where river-breeze-induced NO*x* dilution drives an earlier and more pronounced sensitivity transition. These findings suggest that effective $O_3$ mitigation should combine VOC control throughout the year with coordinated VOC–NO*x* reduction strategies in summer, with particular attention to the spatiotemporal modulation imposed by local meteorological processes.

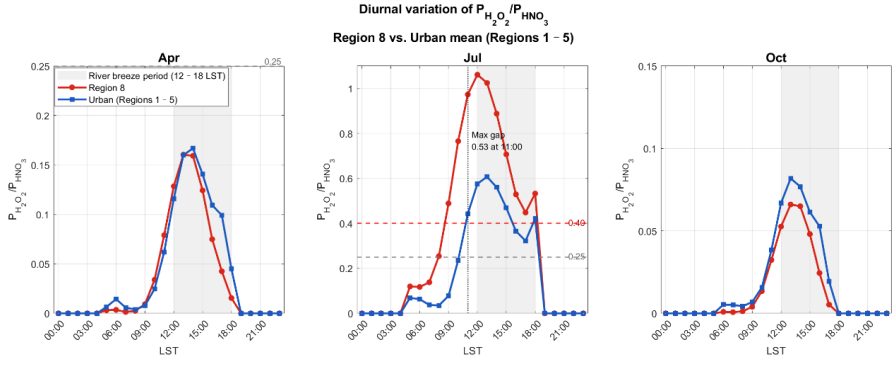


**Figure 8.** Diurnal variation of monthly mean $P_{H_2O_2}/P_{HNO_3}$ for Region 8 (red) and the urban mean (Region 1–5, blue) in April, July, and October. Grey shading marks the peak photochemical period (12:00–18:00 LST). Dashed lines indicate the VOC-limited/Transition (0.25, grey) and Transition/NO*x*-limited boundary (0.40, red) thresholds. The dotted vertical line in July marks the hour of maximum divergence (0.53 at 11:00 LST). January is excluded due to negligible photochemical activity.

https://doi.org/10.5194/egusphere-2026-4158
Preprint. Discussion started: 18 August 2026


## 4. Conclusions

This study investigated the spatial–temporal variability, vertical structure, and driving mechanisms of $O_3$ pollution in the Nanjing section of the Yangtze River using the WRF-CAMx model coupled with SA and PA. By integrating meteorological simulations, emission inventories, and multi-scale analyses, we examined how photochemical processes, boundary-layer dynamics, and terrain-induced circulations jointly regulate $O_3$ distributions in a complex river–valley urban environment.

The results reveal pronounced seasonal and spatial heterogeneity in regional surface $O_3$ concentration, with the Yangtze River corridor showing a dual role as both a transport pathway and an accumulation region depending on seasonal meteorological conditions and boundary-layer structure. The $O_3$ maximum shifts systematically downward from ~5.0 km in winter to ~2.0 km in summer, reflecting intense near-surface photochemical production and efficient vertical mixing in the warm season, in contrast to suppressed boundary-layer development and limited vertical transport in winter. Diurnal variations further demonstrate that boundary-layer evolution plays a central role in regulating the vertical redistribution of $O_3$. Regional diurnal vertical profiles further indicate that land–river thermal contrasts modulate the vertical $O_3$ structure across seasons, with the most pronounced regional differences occurring in summer and the smallest in winter. Together with the contrasting near-surface $O_3$ development over the river corridor and surrounding urban areas, these results indicate that near-surface $O_3$ varies systematically across this complex river–valley terrain and cannot be fully represented by city-averaged characterizations. Cross-sectional analyses reveal that terrain-induced circulations exert fundamental control on the three-dimensional $O_3$ structure. Along the latitudinal transect at 32.032°N, nocturnal stability suppresses near-surface $O_3$ beneath a high-$O_3$ residual layer, while daytime strong updrafts drive an elevated $O_3$ accumulation layer between 0.4 and 1.0 km along the transect. Along the longitudinal transect at 118.842°E, industrial NO*x*–VOC interactions in the Jiangbei sector, local upward transport over the Yangtze River, and terrain-induced upslope lifting over Mt. Zijin collectively highlight the contrasting roles of urban convective forcing and terrain-modulated transport in determining vertical $O_3$

https://doi.org/10.5194/egusphere-2026-4158
Preprint. Discussion started: 18 August 2026


637 distributions across Nanjing.

638 Source apportionment demonstrates that $O_3$ in the Yangtze River corridor is
639 predominantly influenced by regional background transport, while within the locally
640 attributed fraction, Region 8 itself contributes the largest share during daytime, with the
641 highest contribution occurring in April, exceeding 60% and further increasing to 65.2%
642 at 14:00 LST. Seasonal variations reflect shifts in large-scale circulation: northerly
643 winds in winter enhance contributions from the Jiangbei industrial zones (Regions 1
644 and 2, together >34%), while spring and summer favor local recirculation within the
645 river corridor. Under high-$O_3$ episodes, regional transport becomes increasingly
646 dominant, with suburban contributions (Region 7) rising to 45.5% under ≥160 $\mu g/m^3$
647 conditions in July, indicating that extreme pollution events are driven primarily by long-
648 range transport rather than local production. This episode-dependent shift in dominant
649 source regions suggests that source-contribution patterns during high-$O_3$ episodes may
650 differ substantially from those inferred from monthly mean conditions, underscoring
651 the importance of resolving pollution-intensity-dependent changes in regional transport
652 and source attribution.

653 Process analysis demonstrates that $O_3$ variability in the Yangtze River region is
654 governed by coupled chemical–dynamical processes. Diffusion and advection
655 processes play important roles in modulating $O_3$ variability, driven by land–river
656 thermal contrasts and river-breeze circulations, while horizontal advection exhibits a
657 clear diurnal reversal associated with the onset and weakening of the river breeze. These
658 results confirm that $O_3$ in river–valley urban systems follows a coupled chemical–
659 dynamical framework in which photochemistry, boundary-layer processes, and terrain-
660 modulated circulations jointly determine both surface concentrations and vertical
661 distributions.

662 CPA-based sensitivity analysis indicates that $O_3$ production across Nanjing is
663 predominantly VOC-limited throughout the year. In summer, however, the Yangtze
664 River corridor transitions to NO*x*-limited conditions as early as 09:00 LST,
665 approximately two hours ahead of the broader urban area, driven by river-breeze-
666 induced NO*x* dilution. This result suggests that spatially uniform emission control

https://doi.org/10.5194/egusphere-2026-4158
Preprint. Discussion started: 18 August 2026


strategies may be insufficient during summer, and that coordinated VOC–NO*x* reduction measures accounting for local circulation effects are warranted in the river corridor.

Overall, this study highlights the critical role of local circulation systems and terrain effects in shaping the three-dimensional structure of $O_3$ pollution in Nanjing. The findings emphasize that accurate representation of boundary-layer dynamics, land–river thermal contrasts, and terrain-induced flows is essential for understanding, simulating, and mitigating $O_3$ pollution in complex river–valley urban environments, and provide a scientific basis for designing spatially differentiated emission control strategies in regions with similarly complex terrain and circulation systems.

**Funding**

This work was supported by the Zhejiang Provincial Education Department Research Project (Y202455781), Nanxun scholars program of ZJWEU (RC20240101231), and National Natural Science Foundation of China (42307132).

**CRediT authorship contribution statement**

Yan Lu: Writing – review & editing, Writing – original draft, Formal analysis, Visualization, Funding acquisition. Yiming Guo: Software, Data curation. Yan Zhang: Resources, Conceptualization, Data curation. Min Shao: Data curation, Methodology, Supervision, Funding acquisition.

**Declaration of competing interest**

The authors declare that they have no known competing financial interests or personal relationships that could have appeared to influence the work reported in this paper.

**Data availability**

Data will be made available on request.

https://doi.org/10.5194/egusphere-2026-4158
Preprint. Discussion started: 18 August 2026


## Reference

Chen, Z., Xie, Y., Liu, J., Shen, L., Cheng, X., Han, H., Yang, M., Shen, Y., Zhao, T., and Hu, J.: Distinct seasonality in vertical variations of tropospheric ozone over coastal regions of southern China, Science of The Total Environment, 874, 162423, 10.1016/j.scitotenv.2023.162423, 2023.

Cheng, Y., Peng, Y., Cao, L. M., Huang, X. F., and He, L. Y.: Identifying the geospatial relationship of surface ozone pollution in China: Implications for key pollution control regions, Science of The Total Environment, 930, 172763, 10.1016/j.scitotenv.2024.172763, 2024.

Dai, Q., Schulze, B. C., Bi, X., Bui, A. A. T., Guo, F., Wallace, H. W., Sanchez, N. P., Flynn, J. H., Lefer, B. L., Feng, Y., and Griffin, R. J.: Seasonal differences in formation processes of oxidized organic aerosol near Houston, TX, Atmospheric Chemistry and Physics, 19, 9641-9661, 10.5194/acp-19-9641-2019, 2019.

Gong, C., Liao, H., Yue, X., Ma, Y., and Lei, Y.: Impacts of ozone-vegetation interactions on ozone pollution episodes in North China and the Yangtze River Delta, Geophysical Research Letters, 48, 10.1029/2021gl093814, 2021.

Guenther, A., T. Karl, P. Harley, C. Wiedinmyer, P. I. Palmer & C. Geron: Estimates of global terrestrial isoprene emissions using MEGAN (model of emissions of gases and aerosols from nature), Atmospheric Chemistry and Physics, 6(11), 3181–3210. 10.5194/acp-6-3181-2006, 2006.

Guenther, A. B., Jiang, X., Heald, C. L., Sakulyanontvittaya, T., Duhl, T., Emmons, L. K., and Wang, X.: The Model of Emissions of Gases and Aerosols from Nature version 2.1 (MEGAN2.1): An extended and updated framework for modeling biogenic emissions, Geoscientific Model Development, 5, 1471-1492, 10.5194/gmd-5-1471-2012, 2012.

Guo, W., Yang, Y., Zhang, J., Han, K., Yang, Y., Chen, Q., Li, S., and Zhu, Y.: Effects of valley topography on ozone pollution in the Lanzhou valley: A numerical case study, Environmental Pollution, 363, 125225, 10.1016/j.envpol.2024.125225, 2024.

Hou, X., Wang, X., Cheng, S., Qi, H., Wang, C., and Huang, Z.: Elucidating transport dynamics and regional division of $PM_{2.5}$ and $O_3$ in China using an advanced network model, Environment International, 188, 108731, 10.1016/j.envint.2024.108731, 2024.

Huszar, P., Karlický, J., Marková, J., Nováková, T., Liaskoni, M., and Bartík, L.: The regional

https://doi.org/10.5194/egusphere-2026-4158
Preprint. Discussion started: 18 August 2026


impact of urban emissions on air quality in Europe: the role of the urban canopy effects, Atmospheric Chemistry and Physics, 21, 14309-14332, 10.5194/acp-21-14309-2021, 2021.

Li, M., Liu, H., Geng, G., Hong, C., Liu, F., Song, Y., Tong, D., Zheng, B., Cui, H., Man, H., Zhang, Q., and He, K.: Anthropogenic emission inventories in China: A review, National Science Review, 4, 834-866, 10.1093/nsr/nwx150, 2017.

Li, T., Wu, N., Chen, J., Chan, P.-w., Tang, J., and Wang, N.: Vertical exchange and cross-regional transport of lower-tropospheric ozone over Hong Kong, Atmospheric Research, 292, 106877, 10.1016/j.atmosres.2023.106877, 2023.

Li, X., Qin, M., Li, L., Gong, K., Shen, H., Li, J., and Hu, J.: Examining the implications of photochemical indicators for $O_3$–NO*x*–VOC sensitivity and control strategies: A case study in the Yangtze River Delta (YRD), China, Atmospheric Chemistry and Physics, 22, 14799-14811, 10.5194/acp-22-14799-2022, 2022.

Li, X. B., Fan, G., Lou, S., Yuan, B., Wang, X., and Shao, M.: Transport and boundary layer interaction contribution to extremely high surface ozone levels in eastern China, Environmental Pollution, 268, 115804, 10.1016/j.envpol.2020.115804, 2021.

Liu, K., Wang, H., Gong, X., Li, Y., Wang, J., Lu, M., Tang, X., Xue, C., Peng, J., Song, S., Zhang, Y., and Feng, Y.: Shifts of the three-dimensional $O_3$ photochemical regime of the North China Plain within the boundary layer, Environmental Science & Technology Letters, 12, 1197-1204, 10.1021/acs.estlett.5c00741, 2025.

Lu, Y., Wu, Z., Pang, X., Wu, H., Xing, B., Li, J., Xiang, Q., Chen, J., and Shi, D.: Temporal characteristics of ozone ($O_3$) in the representative city of the Yangtze River Delta: Explanatory factors and sensitivity analysis, International Journal of Environmental Research and Public Health, 20, 10.3390/ijerph20010168, 2022.

Luo, Z., Han, Y., Hua, K., Zhang, Y., Wu, J., Bi, X., Dai, Q., Liu, B., Chen, Y., Long, X., and Feng, Y.: The effect of emission source chemical profiles on simulated $PM_{2.5}$ components: Sensitivity analysis with the Community Multiscale Air Quality (CMAQ) modeling system version 5.0.2, Geoscientific Model Development, 16, 6757-6771, 10.5194/gmd-16-6757-2023, 2023.

Lyu, Y., Xu, H., Wu, H., Han, F., Lv, F., Kang, A., and Pang, X.: Spatiotemporal variations of $PM_{2.5}$ and ozone in urban agglomerations of China and meteorological drivers for ozone using explainable machine learning, Environmental Pollution, 365, 125380,

https://doi.org/10.5194/egusphere-2026-4158
Preprint. Discussion started: 18 August 2026


10.1016/j.envpol.2024.125380, 2025a.

Lyu, Y., Wu, D., Han, F., Zhang, H., Lv, F., Kang, A., Hu, Y., and Pang, X.: Co-occurring extremes of $PM_{2.5}$ and ozone in warm seasons of the Yangtze River Delta of China: Insights from explainable machine learning, ACS ES&T Air, 2, 578-588, 10.1021/acsestair.4c00314, 2025b.

Mao, Y. H., Shang, Y., Liao, H., Cao, H., Qu, Z., and Henze, D. K.: Sensitivities of ozone to its precursors during heavy ozone pollution events in the Yangtze River Delta using the adjoint method, Science of The Total Environment, 925, 171585, 10.1016/j.scitotenv.2024.171585, 2024.

Qi, C., Wang, P., Yang, Y., Li, H., Zhang, H., Ren, L., Jin, X., Zhan, C., Tang, J., and Liao, H.: Impacts of tropical cyclone–heat wave compound events on surface ozone in eastern China: Comparison between the Yangtze River and Pearl River deltas, Atmospheric Chemistry and Physics, 24, 11775-11789, 10.5194/acp-24-11775-2024, 2024.

Quimbayo-Duarte, J., Chemel, C., Staquet, C., Troude, F., and Arduini, G.: Drivers of severe air pollution events in a deep valley during wintertime: A case study from the Arve river valley, France, Atmospheric Environment, 247, 118030, 10.1016/j.atmosenv.2020.118030, 2021.

Shao, M., Lv, S., Wei, Y., and Zhu, J.: The various synergistic impacts of precursor emission reduction on $PM_{2.5}$ and $O_3$ in a typical industrial city with complex distributions of emissions, Science of The Total Environment, 940, 173497, 10.1016/j.scitotenv.2024.173497, 2024a.

Shao, M., Liu, X., Lv, S., Dai, Q., and Mu, Q.: The importance of local thermal circulations in $PM_{2.5}$ formation in a river valley: A case study from the lower Yangtze River, China, Journal of Geophysical Research: Atmospheres, 129, 10.1029/2023jd039717, 2024b.

Shi, L., Zhu, A., Huang, L., Yaluk, E., Gu, Y., Wang, Y., Wang, S., Chan, A., and Li, L.: Impact of the planetary boundary layer on air quality simulations over the Yangtze River Delta region, China, Atmospheric Environment, 263, 118685, 10.1016/j.atmosenv.2021.118685, 2021.

Sillman, S.: The use of NOy, $H_2O_2$ and $HNO_3$ as indicators for ozone-NOx-hydrocarbon sensitivity in urban locations, Journal of Geophysical Research: Atmospheres, 100, 14175-14188, 1995.

Skamarock, C., Klemp, B., Dudhia, J., Gill, O., Liu, Z., Berner, J., et al.: A description of the advanced research WRF model version 4. National Center for Atmospheric Research. 10.5065/1DFH-6P97, 2019.

https://doi.org/10.5194/egusphere-2026-4158
Preprint. Discussion started: 18 August 2026


787 Song, Y. and Shao, M.: Impacts of complex terrain features on local wind field and $PM_{2.5}$
788 concentration, Atmosphere, 14, 761, 10.3390/atmos14050761, 2023.
789 Sueki, K., Yamaura, T., Yashiro, H., Nishizawa, S., Yoshida, R., Kajikawa, Y., and Tomita, H.:
790 Convergence of convective updraft ensembles with respect to the grid spacing of atmospheric
791 models, Geophysical Research Letters, 46, 14817-14825, 10.1029/2019gl084491, 2019.
792 Tian, J., Wang, J., Wang, D., and Fang, C.: Influence of urbanization on meteorological conditions
793 and ozone pollution in the Central Plains Urban Agglomeration, China, Environmental
794 Pollution, 356, 124290, 10.1016/j.envpol.2024.124290, 2024.
795 Vermeuel, M. P., Novak, G. A., Alwe, H. D., Hughes, D. D., Kaleel, R., Dickens, A. F., Kenski, D.,
796 Czarnetzki, A. C., Stone, E. A., Stanier, C. O., Pierce, R. B., Millet, D. B., and Bertram, T. H.:
797 Sensitivity of ozone production to NO*x* and VOC along the Lake Michigan Coastline, Journal
798 of Geophysical Research: Atmospheres, 124, 10989-11006, 10.1029/2019jd030842, 2019.
799 Von Storch, H., H. Langenberg, F. Feser: A spectral nudging technique for dynamical downscaling
800 purposes. Monthly Weather Review, 128(10), 3664–3673, 2000.
801 Wang, Y., Yaluk, E. A., Chen, H., Jiang, S., Huang, L., Zhu, A., Xiao, S., Xue, J., Lu, G., Bian, J.,
802 Kasemsan, M., Zhang, K., Liu, H., Tong, H., Ooi, M. C. G., Chan, A., and Li, L.: The
803 importance of NO*x* control for peak ozone mitigation based on a sensitivity study using
804 CMAQ-HDDM-3D model during a typical episode over the Yangtze River Delta region, China,
805 Journal of Geophysical Research: Atmospheres, 127, 10.1029/2022jd036555, 2022.
806 Wei, W., Lv, Z. F., Li, Y., Wang, L. T., Cheng, S., and Liu, H.: A WRF-Chem model study of the
807 impact of VOCs emission of a huge petro-chemical industrial zone on the summertime ozone
808 in Beijing, China, Atmospheric Environment, 175, 44-53, 10.1016/j.atmosenv.2017.11.058,
809 2018.
810 Wu, L. and An, J.: Quantitative impacts of meteorology and emissions on the long-term trend of $O_3$
811 in the Yangtze River Delta (YRD), China from 2015 to 2022, Journal of Environmental
812 Sciences (China), 149, 314-329, 10.1016/j.jes.2024.01.038, 2025.
813 Xu, J., Huang, X., Wang, N., Li, Y., and Ding, A.: Understanding ozone pollution in the Yangtze
814 River Delta of eastern China from the perspective of diurnal cycles, Science of The Total
815 Environment, 752, 141928, 10.1016/j.scitotenv.2020.141928, 2021.
816 Zhang, H., Lv, L., Yao, Z., Guo, W., Wang, X., Shan, W., Li, X., and Shen, X.: Vertical variations of

https://doi.org/10.5194/egusphere-2026-4158
Preprint. Discussion started: 18 August 2026


817 ozone transport flux at multiple altitudes and identification of major transport direction in the
818 North China Plain, Journal of Environmental Sciences (China), 155, 488-500,
819 10.1016/j.jes.2024.05.046, 2025a.
820 Zhang, J., Li, D., Bian, J., Xuan, Y., Chen, H., Bai, Z., Wan, X., Zheng, X., Xia, X., and Lü, D.:
821 Long-term ozone variability in the vertical structure and integrated column over the North
822 China Plain: Results based on ozonesonde and Dobson measurements during 2001–2019,
823 Environmental Research Letters, 16, 074053, 10.1088/1748-9326/ac109f, 2021.
824 Zhang, S., Yuan, Z., Zheng, Z., and Zhao, K.: Quantitative impacts of dominant large-scale
825 circulation systems on surface ozone pollution in China, Journal of Environmental Sciences
826 (China), 156, 42-55, 10.1016/j.jes.2024.07.015, 2025b.
827 Zhang, Y., Zhang, F., Wan, M., Bo, Y., He, K., and Liu, R.: Evolution of surface ozone pollution in
828 Yangtze Rriver Delta between 2019 and 2022: Influences of meteorology and emissions,
829 Atmospheric Environment, 358, 121339, 10.1016/j.atmosenv.2025.121339, 2025c.
830 Zhang, Y., Wang, H., Lu, X., Li, L., He, Y., Wang, H., He, G., He, C., Wang, J., and Fan, S.: Evolution
831 of summer surface ozone pollution patterns in China during 2015–2020, Atmospheric Research,
832 291, 106836, 10.1016/j.atmosres.2023.106836, 2023.
833 Zheng, B., Huo, H., Zhang, Q., Yao, Z. L., Wang, X. T., Yang, X. F., Liu, H., and He, K. B.: High-
834 resolution mapping of vehicle emissions in China in 2008, Atmospheric Chemistry and Physics,
835 14, 9787-9805, 10.5194/acp-14-9787-2014, 2014.
836